Chemical Science

EDGE ARTICLE

View Article Online
View Journal | View Issue

Cite this: *Chem. Sci.*, 2015, **6**, 6256

In vivo visualization of osteoarthritic hypertrophic lesions†

Hai-Yu Hu,[abe] Ngee-Han Lim,[c] Hans-Paul Juretschke,[b] Danping Ding-Pfennigdorff,[b] Peter Florian,[b] Markus Kohlmann,[b] Abdullah Kandira,[b] Jens Peter von Kries,[b] Joachim Saas,[b] Karl A. Rudolphi,[b] K. Ulrich Wendt,[b] Hideaki Nagase,[b] Oliver Plettenburg,[b] Marc Nazare*[bd] and Carsten Schultz*[a]

Received 10th April 2015
Accepted 12th August 2015

DOI: 10.1039/c5sc01301a

www.rsc.org/chemicalscience

Osteoarthritis (OA) is one of the most common diseases in the aging population. While disease progress in humans is monitored indirectly by X-ray or MRI, small animal OA lesions detection always requires surgical intervention and histology. Here we introduce bimodal MR/NIR probes based on cartilage-targeting 1,4,7,10-tetraazacyclododecane 1,4,7,10-tetraacetic acid amide (DOTAM) that are directly administered to the joint cavity. We demonstrate applications in healthy and diseased rat joints by MRI *in vivo*. The same joints are inspected post-mortem by fluorescence microscopy, showing not only the precise location of the reagents but also revealing details such as focal cartilage damage and chondrophyte or osteophyte formation. This allows for determining the distinct pathological state of the disease and the regeneration capability of the animal model and will help to correctly assess the effect of potential disease modifying OA drugs (DMOADs) in the future.

Introduction

Osteoarthritis is a slowly developing, chronic degenerative disease mainly characterized by destruction of joint cartilage,[1] which inflicts severe pain and disability on patients. A major limitation in developing new therapies is the lack of optimally predictive small animal models.[2] In current models, development of disease pathology can only be assessed by post-mortem histological examination; additionally, the disease phenotypes are extremely heterogeneous, resulting in high subgroup variability at early timepoints in particular (see ESI S1†) and hampering the precise characterization of new DMOADs in interventional studies. To allow the latter, non-invasive characterization of disease state of individual animals before and during treatment would represent a major improvement in the performance of pharmacological research and result in a significant reduction in the number of animals used per study.

Non-invasive imaging techniques of choice are micro-computed tomography[3–5] and magnetic resonance imaging (MRI).[6–13] However, articular cartilage of the knee joint is avascular and the encapsulation by the synovial membrane further prevents the access of contrast agents. In addition, the effective local administration of agents *via* intra-articular injection into the joint space is hampered by rapid clearance through convective transport and lymphatic drainage leading to short residence time of low molecular weight solutes between one to two hours.[14–16] Detection of subtle pathological changes in cartilage morphology during disease, such as focal cartilage damage and chondrophytes or osteophyte formation will improve evaluation of pharmacological studies, which requires highly sensitive imaging probes.[8,17–19] Chondrophytes are areas of hypertrophic cartilage that form at the edges of the joint surface which becomes vascularized and transforms into bone tissue (osteophytes) in advanced disease,[20,21] the latter being the hallmark in the radiographic diagnosis of OA.

There is a strong need for better imaging tools to detect OA lesions and to visualize the progression of disease stage in experimental animal disease models over time (ESI S1†). In this context, charged gadolinium contrast agents were reported for delayed gadolinium enhanced magnetic resonance imaging of cartilage (dGEMRIC), which rely on Coulomb interactions between the cationic ionic contrast agents and the highly

[a]*European Molecular Biology Laboratory (EMBL), Interdisciplinary Chemistry Group, Cell Biology and Biophysics Unit, Meyerhofstr. 1, 69117 Heidelberg, Germany. E-mail: schultz@embl.de*

[b]*Sanofi-Aventis Deutschland GmbH, Industriepark Hoechst, 65962 Frankfurt, Germany*

[c]*Kennedy Institute of Rheumatology, University of Oxford, Roosevelt Drive, Headington, Oxford OX37FY, UK*

[d]*Leibniz-Institut für Molekulare Pharmakologie (FMP), Campus Berlin-Buch, Robert-Roessle-Str. 10, 13125 Berlin, Germany. E-mail: nazare@fmp-berlin.de*

[e]*State Key Laboratory of Bioactive Substance and Function of Natural Medicines, Institute of Materia Medica, Peking Union Medical College and Chinese Academy of Medical Sciences, 1 Xiannongtan Street, 100050, Beijing, China*

† Electronic supplementary information (ESI) available: Supplemental figures, synthetic schemes, experimental procedures, characterization of all new compounds, histopathological scoring of joint damage in the rat ACLT-pMx OA model, detailed *ex vivo*MRI studies with pig cartilage explants, *in vivo* MRI studies with rats, immunofluorescence staining for procollagen type IIA. See DOI: 10.1039/c5sc01301a

negatively charged glycosaminoglycan (GAG) polysaccharides resulting in a tissue distribution inversely related to the negatively-charged GAG content.[6,22–24] Here we report for the first time the design and synthesis of small molecule based near-infrared fluorescence and gadolinium-based T_1 MRI contrast agents that bind specifically to cartilage and demonstrate efficacy to visualize cartilage regions in healthy and diseased rat joints by MRI *in vivo*. This allows the assessment of distinct disease states in a model of OA in rats with surgically-induced knee joint instability by anterior cruciate ligament transection and partial (~25%) meniscectomy (ACLT-pMx).[25] The same probes are investigated histologically and by fluorescence at the end of the experiment.

Results and discussion

In vivo probe design and synthesis

Articular cartilage is a highly functional tissue which covers the ends of long bones and serves to ensure proper joint movement. It is comprised of two main extracellular components, type II collagen and GAGs.[26] Therefore, we hypothesized that contrast agents capable of binding collagen II and GAGs would improve imaging resolution sufficiently to study cartilage biology and disease. Hubbell *et al.* have shown that functionalized nanoparticles with the specific peptide sequence, WYRGRL, exhibiting high affinity for collagen type II α1, thus targeting articular cartilage well.[27] We reported that an equal cartilage retention can be achieved *in vivo* by the AcWYRGRL-DOTAM conjugate without using pluronic-based nanoparticles.[28] Additionally, cationic moieties are known to electrostatically attach to anionic GAGs.[3,29,30] To generate a high T_1 relaxivity probe for molecular imaging of cartilage *in vivo* by MRI, a DOTAM[31,32] backbone was selected as a template, which offers the advantage of being easily functionalized with conformationally flexible arm moieties and allowing for a multivalent decoration with collagen II targeting peptides and GAG-targeting amino groups. This constellation was expected to retain the chelating properties for Gd^{3+} ions forming kinetically stable complexes.[33] The DOTAM template is easy to synthesize, cost effective, and non-toxic. DOTAM is easily functionalized and has metal ion binding properties and biocompatibility.[34] However, a strategy to directly use DOTAM as a multivalent template for dual targeting and as an MRI contrast agent has to the best of our knowledge not been reported yet.

Compound **1** was prepared in 6 steps from cyclen (Scheme 1). The acetylated collagen II binding peptide AcWYRGRL was synthesized by standard solid-phase peptide synthesis and then attached to **1** after Fmoc deprotection. Three GAG targeting terminal amino groups were introduced by the deprotection of the Boc groups. The corresponding Gd(III) complex, termed cartilage targeting contrast agent (**TCA**), was formed by incubation with $GdCl_3$ at pH 6 for 48 h (detailed procedures for the syntheses are provided in the ESI†). The control compound, non-targeting contrast agent (**NCA**), featured a scrambled peptide sequence and acetylated terminal amino groups.

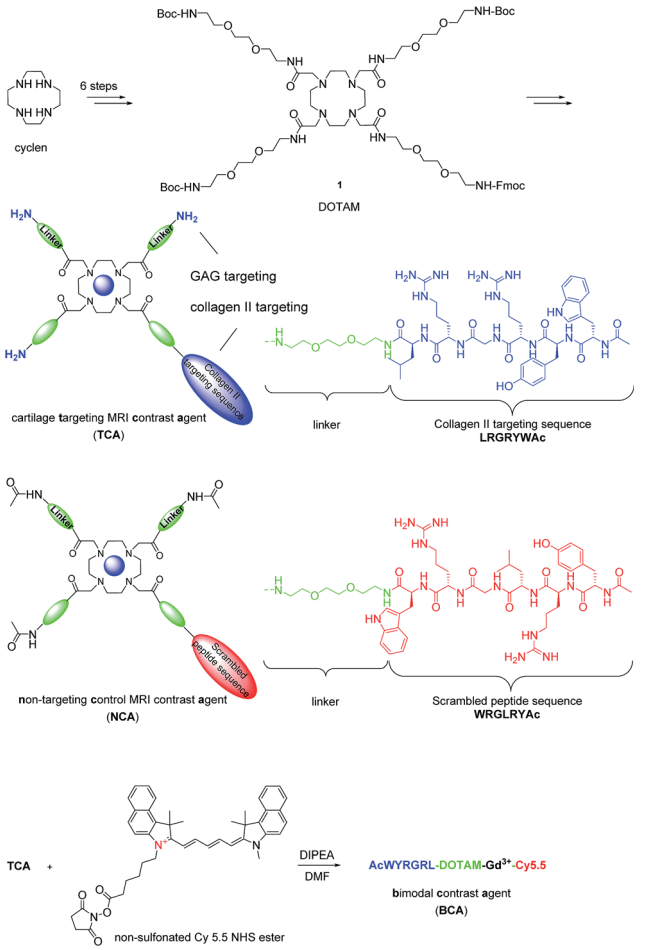

Scheme 1 Synthesis of MRI contrast agents based on DOTAM. For a more detailed description of the chemistry, see the ESI.†

Probe characterization *in vitro*

The T_1 signal enhancement of the targeting contrast agent **TCA** in DPBS (Dulbecco's phosphate-buffered saline) buffer was measured and compared with Gd-DTPA (Gd-diethylenetriamine pentaacetic acid), a commercially available contrast agent in clinical use (see ESI Fig. S2†).[35] Due to slower water exchange in the amide-containing complexes,[36] the longitudinal relaxivity value r_1 found for **TCA** ($r_1 = 1.6\ mM^{-1}\ s^{-1}$) is lower than that of Gd-DTPA ($r_1 = 3.9\ mM^{-1}\ s^{-1}$, $T_1 = 887 \pm 7$ ms, 0.2 mM). However, **TCA** was an effective T_1 signal enhancer ($T_1 = 1492 \pm 12$ ms, 0.2 mM), capable of reducing the bulk water T_1 ($T_1 = 2843 \pm 63$ ms) by 47%. *In vitro* **TCA** and **NCA** were stable at pH > 2 with no detectable dissociation at 24 h during incubation with TFA; although DOTAM complexes were reported to be considerably less stable than the corresponding $[M(DOTA)]^{2-}$ complexes, largely due to the lower basicity of the tetraamide ligands.[37]

Ex vivo probe characterization

To evaluate the ability of the contrast agent **TCA** to image articular cartilage, we investigated pig articular cartilage explants using MRI and employing Gd-DTPA as a reference. In these *ex vivo* experiments, whole-depth pig articular cartilage

blocks were incubated with 0.2 mM **TCA** or Gd-DTPA at 37 °C for 24 h, washed three times for 10 min each with DPBS buffer at 37 °C to remove free contrast agent, then imaged by MRI. The images obtained from pig articular cartilage explants studies ($n = 4$) showed an unambiguous signal enhancement when using **TCA** (ESI Fig. S3†) compared to Gd-DTPA (T_1: 430 ± 16 ms *vs.* 1403 ± 5 ms). The level of signal enhancement demonstrates the high effectiveness of the cartilage targeting property of **TCA** for the visualization by MRI.

Probe characterization *in vivo*

MRI is the most common non-invasive tool used *in vivo* to assess intra-articular soft tissues, and cartilage in particular. However, for small animals such as rats the assessment of cartilage lesions is highly challenging due to the small size of the knee joint as the articular cartilage is only 0.5 mm thick and for Gd-DTPA, also, a rapid clearance from the joint after intra-articular injection was observed.[8,38] Enhancement of the MRI contrast with **TCA** would improve the evaluation of articular cartilage damage. **NCA** containing the non-binding scrambled peptide sequence YRLGRW ($r_1 = 1.9$ mM^{-1} s^{-1}, 25 °C in DPBS) (see ESI Fig. S2†) was used as a control agent, initially in healthy rats ($n = 4$).

The *in vivo* cartilage targeting capability of the contrast agents was visualized and estimated by injecting **TCA** and **NCA** each in one knee of the same rat, which allowed direct comparison of labeling and clearance behavior of the two different contrast agents over time without background by interanimal differences.[39] We observed a rapid clearance of both contrast agents from non-cartilage compartments of the joint such as meniscus, synovium, fat tissues, muscles, and bones within 4 hours (see ESI Fig. S5–S8†). Fig. 1a shows a representative image obtained 24 hours after intra-articular injection of both contrast agents. A significant MRI signal enhancement of the articular cartilage and growth plate which consist primarily of collagen II and proteoglycan was detected in the **TCA** applied knees. The signal intensities (SIs) in the articular cartilage and growth plate increased by 86% ($^*P < 0.05$) and 77% ($^{**}P < 0.001$) after 24 hours and 84% ($^{**}P < 0.001$) and 85% ($^{***}P < 0.0001$) after 72 hours, respectively, following administration of **TCA** (Fig. 1b) while the signal was totally cleared within 72 hours in **NCA** injected knees. This confirmed that the MRI signal enhancement of the articular and growth plate cartilage is due to the specific tissue targeting of **TCA**. These results are fully in line with earlier results where the collagen II targeting moiety provided significant improvement through the cartilage targeting effect over the Coulomb interactions driven GAG targeting moieties. Targeting *via* cationic moieties only showed a weak improvement over the none-targeting control.[28]

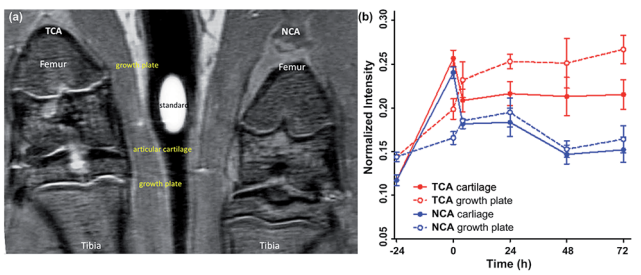

Fig. 1 (a) MR images of rat knees 24 hours after injection of contrast agents **TCA** (left) and **NCA** (right), (b) plots of normalized intensities (mean ± standard error, $n = 4$) before and after injection of **TCA** and **NCA** (cartilage and growth plate).

Detection of lesions *in vivo* and validation by histology

Following the demonstration of the specificity of cartilage binding of **TCA** *in vivo* with healthy rats, we next set out to investigate if OA cartilage lesions could be visualized by **TCA** in an animal model. Although there is in depth knowledge about the different disease stages, pathologies based on histological examinations, and subsequent scoring procedures, there is no satisfactory method available for visualization of these processes *in vivo*.

To investigate the imaging properties of the probes in diseased animals, we subjected rats to ACLT-pMx. One knee was surgically destabilized while the other was left untouched to serve as internal control, and images were taken 28 days after surgery ($n = 4$). As we intended to later visualize probe location by fluorescence, we decided to co-administer a bimodal probe, BCA ($r_1 = 1.6$ mM^{-1} s^{-1}, 25 °C in DPBS), resulting from the conjugation of TCA with the fluorophore Cy 5.5. In order to reduce the interference of GAG targeting affinity, Cy 5.5 with one positive charge was used, keeping the net charge of the probe unchanged. Taking into account the different sensitivities of optical and MRI based imaging, TCA/BCA (50 μL of a 10 mM DPBS solution of 1% BCA and 99% TCA) was injected intra-articularly into the right knees which had undergone

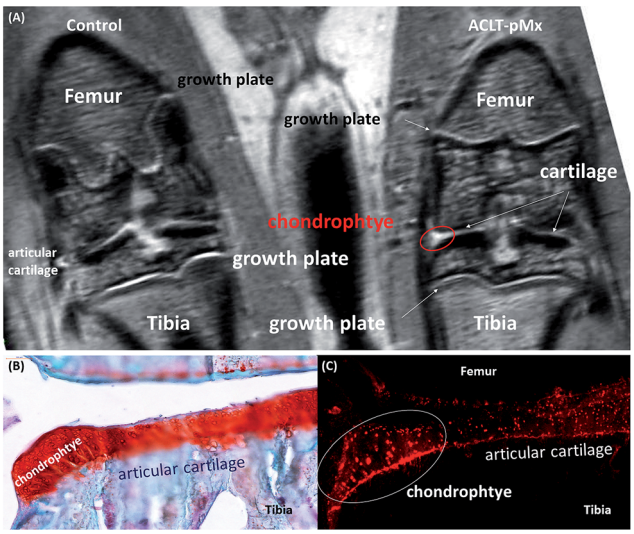

Fig. 2 (A) *In vivo* MR images of injured *vs.* non-operated control rat knees 24 hours after co-injection of contrast agents **TCA** and **BCA**. (B) Photomicrograph of medial aspect of the ACLT-pMx knee joint slice, stained with Safranin O and counterstained with Fast Green. (C) Fluorescent image of the consecutive ACLT-pMx knee joint slice from the same stack ($\lambda_{em} = 695$ nm).

surgery, as well as into the left control knees ($n = 4$). Images were taken immediately after administration and probe localization was followed over 2 days (Fig. 2A). In the non-operated knee joints, a clear MRI signal enhancement of articular cartilage and growth plate compared to the operated knee was observed. In addition to the expected increase of signal intensity of the articular cartilage, we observed a region with significantly brighter MRI signal in the medial tibial plateau of the ACLT-pMx knee (Fig. 2A, red circle), which could indicate a region of compensatory hypertrophy.

The MRI results were further confirmed by standard histology. The ACLT-pMx model rats were sacrificed at 48 h post-administration and the knee joints excised, frozen, and sectioned for histologic analysis. Chondrophyte and osteophyte regions were examined in sections stained with Safranin O/Fast Green and recorded using a Zeiss Miraxscan microscope (Fig. 2B). The non-operated joints exhibited no chondrophytes or osteophyte formation in the femoral condyles or the tibial plateau while the ACLT-pMx joints showed early chondrophytes, pre-osteophyte (stage I), formation at the margin of the medial tibial plateau. These results are in very good accordance with the disease staging information obtained in the previously described longitudinal study (ESI S1†).

Fluorescence microscopy of the sectioned knee slices revealed a high level of fluorescence signal in the cartilage tissue (Fig. 2C), which is in agreement with the MRI data and shows the selective and high degree of accumulation of the probes in the cartilage tissue due to the intrinsic targeting effect. Besides the cartilage areas of the ACLT-pMx joint, a strong signal was obtained at the chondrophyte pre-osteophyte area, which might result from the expression of GAGs as well as collagen IIA (for immunofluorescence staining of the diseased knee, see Fig. S10 in the ESI†), a splice variant of collagen II expressed by chondroprogenitor cells, at early chondrophytes and osteophytes.[20] However, the exact binding mechanism of BCA to chondrophytes remains to be further elucidated. In the non-operated knee joint, no sign of hypertrophy in the cartilage was observed. The probe was distributed homogeneously within articular cartilage (Fig. 3). NIRF signals were observed both in the matrix compartment and within chondrocytes. The pericellular matrix and the cell nuclei were free of signal (Fig. 3, ESI S9†).

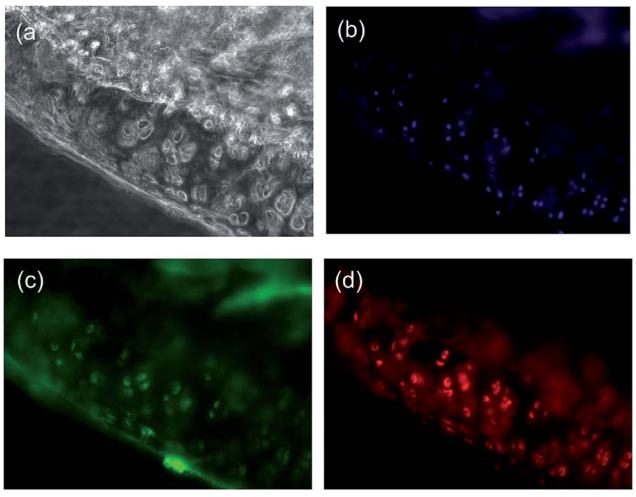

Fig. 3 Probe distribution in articular cartilage of the non-operated control knee joint after 48 h. (a) Wide field imaging, (b) DAPI nuclear stain, (c) Perlecan stain (the edges of pericellular matrix), (d) BCA Cy 5.5 channel.

Conclusions

The frequently used surgically-induced ACLT-pMx animal model in rats suffers from the fact that the degree of joint damage is highly variable, thus requiring a relatively large number of animals for pharmaco-therapeutic studies (as an example, see Fig. S1†). This may be significantly reduced by applying non-invasive imaging *in vivo*, although the small dimensions of rat joints and the limited contrast of conventional MRI are so far insufficient to truly detect defects of articular cartilage in small rodents. With our novel MRI contrast agent TCA, we were able to clearly observe formation of chondrophytes which are bulges of metaplastic, hypertrophic cartilage forming the edges of the articular cartilage layer early in OA pathogenesis. Later in the disease process, chondrophytes become vascularized, calcify, and transform into osteophytes.[21] Osteophyte presence is detectable by conventional X-radiography and an important component in the well-established Kellgren–Lawrence radiographic diagnostic tool.[40] Importantly, their location and size significantly correlates with the degree of cartilage destruction,[41] and also with clinical severity of OA symptoms such as pain.[42] Therefore chondrophyte and pre-osteophyte formation represents a hallmark of OA pathogenesis and a well-suited timepoint for initiation of a therapeutic intervention.

We have developed the first active cartilage-targeting Gd-based MRI contrast agent that selectively localizes in collagenous cartilage and is able to detect early chondrophytes or pre-osteophyte formation *in vivo* in an experimental rat model of OA. The chemical design is based on the easily accessible multivalency of the DOTAM core which provides excellent possibilities for using various linkers, peptides, and fluorophores. In addition, the successful probe targeting demonstrated here might be a new starting point for developing locally acting drug candidates. As a bimodal probe, BCA enabled us to localize and characterize chondrophyte and pre-osteophyte formation through correlation of *in vivo* MRI and *in vitro* fluorescence data. We expect that the use of such active targeting principles attached to the described DOTAM/Gd-platform will be generally useful for the site specific MRI contrast enhancement of other complex avascular or collagen-rich tissues. Further, different targeting mechanisms are easily incorporated by introducing single or multiple peptide copies to fine tune binding affinity and tissue selectivity.

Preclinical application of these collagen-targeting agents will lead to a better understanding of the development stage of disease pathology in individual animals thus paving the way for the early detection of OA in humans. In particular in slowly developing chronic diseases such as osteoarthritis, it may

become extremely valuable to allow classifying and grouping of animals by reaching a given disease state. This will result in significantly reduced variability and thus will improve the process of probing new pharmaceutical principles by generating statistically more meaningful data at early points in time. At the same time, the number of animals required per study will decrease substantially. Further studies demonstrating the utility of this method for profiling of novel therapeutics will be performed in the future.

Experimental section

General procedures for solid-phase peptide synthesis

The peptides WYRGRL and YRLGRW were synthesized on solid resin using an automated peptide synthesizer (CEM Microwave Peptide Synthesizer) with standard Fmoc chemistry. Both of the peptides were acetylated at the N terminus with a large excess of acetic anhydride and DIPEA. The fully protected peptide was cleaved from the resin using 30% HFIP in DCM and characterized by LC-MS.

Gadolinium complex formation

Complexes were prepared by adding a 1 mM $GdCl_3$ stock solution to a DOTA-peptide ligand solution, in stoichiometric amounts (1 : 1). The pH was adjusted to 6 using 1 N NaOH and stirred for 48 h and then centrifuged to remove any precipitated $Gd(OH)_3$. The presence of free Gd^{3+} was evaluated by colorimetry using xylenolorange as an indicator. Resultant peptide complexes were further purified by HPLC. The purified complex solution was lyophilized to give the gadolinium complex as a powder solid. **TCA** HRMS calcd for $C_{82}H_{143}N_{25}O_{20}Gd$: 1956.01656; found: 1956.01628 ($[M + H]^{4+} = 489.25589$); **NCA** ESI-MS calcd for $C_{88}H_{149}N_{25}O_{23}Gd$: 2082.57; found: 2083.4 ($[M + H]^{4+} = 521.1$).

Synthesis of bimodal cartilage-targeted imaging probesBCA

TCA (19 mg, 10 μmol) was dissolved in 1.5 ml DMF, followed by the addition of 1 equiv. Cy 5.5 NHS ester (7 mg, 10 μmol) and 5 equiv. DIPEA (10 μl, 50 μmol). The reaction mixture was stirred under argon at room temperature for 12 hours. After the reaction was complete, the reaction solution was directly purified by HPLC to give to give **BCA** (13 mg, yield 51%) as a blue powder. HRMS calcd for $C_{122}H_{184}N_{28}O_{20}Gd$: 2521.33792; found: 2521.33802 ($[M + H]^{4+} = 504.46906$).

Author contributions

H.-Y. H., M. N., and C. S. conceived the idea and designed the experiments. H.-Y. H., H. P. J., and K. A. R. performed experiments with the help of D. D.-P., M. K., A. K., J. P. K., J. S., and J. P. K. H.-Y. H. conducted the data analysis with the help from D. D.-P., P. F., K. A. R., and N.-H. L. H.-Y. H., M. N., O. P., N.-H. L., and C. S. wrote the manuscript with input from all authors. K. U. W., O. P., H. N., M. N., and C. S. supervised research.

Acknowledgements

All authors acknowledge funding by LIVIMODE, a collaborative FP7 project of the EU.

Notes and references

1 H. A. Wieland, M. Michaelis, B. J. Kirschbaum and K. A. Rudolphi, *Nat. Rev. Drug Discovery*, 2005, **4**, 331–344.
2 E. Teeple, G. Jay, K. Elsaid and B. Fleming, *AAPS J.*, 2013, **15**, 438–446.
3 N. S. Joshi, P. N. Bansal, R. C. Stewart, B. D. Snyder and M. W. Grinstaff, *J. Am. Chem. Soc.*, 2009, **131**, 13234–13235.
4 I. O. Afara, I. Prasadam, R. Crawford, Y. Xiao and A. Oloyede, *Bone*, 2013, **53**, 350–357.
5 D. Pan, E. Roessl, J.-P. Schlomka, S. D. Caruthers, A. Senpan, M. J. Scott, J. S. Allen, H. Zhang, G. Hu, P. J. Gaffney, E. T. Choi, V. Rasche, S. A. Wickline, R. Proksa and G. M. Lanza, *Angew. Chem., Int. Ed.*, 2010, **49**, 9635–9639.
6 D. J. Hunter and A. Guermazi, *Phys. Med. Rehabil.*, 2012, **4**, S68–S74.
7 J. C. Goebel, R. Bolbos, M. Pham, L. Galois, A. Rengle, D. Loeuille, P. Netter, P. Gillet, O. Beuf and A. Watrin-Pinzano, *Rheumatology*, 2010, **49**, 1654–1664.
8 J. C. Goebel, A. Pinzano, D. Grenier, A. L. Perrier, C. Henrionnet, L. Galois, P. Gillet and O. Beuf, *Bio-Med. Mater. Eng.*, 2010, **20**, 189–194.
9 P. Caravan, B. Das, S. Dumas, F. H. Epstein, P. A. Helm, V. Jacques, S. Koerner, A. Kolodziej, L. Shen, W.-C. Sun and Z. Zhang, *Angew. Chem., Int. Ed.*, 2007, **46**, 8171–8173.
10 E. Boros, M. Polasek, Z. Zhang and P. Caravan, *J. Am. Chem. Soc.*, 2012, **134**, 19858–19868.
11 R. Uppal, K. L. Ciesienski, D. B. Chonde, G. S. Loving and P. Caravan, *J. Am. Chem. Soc.*, 2012, **134**, 10799–10802.
12 R. C. Strauch, D. J. Mastarone, P. A. Sukerkar, Y. Song, J. J. Ipsaro and T. J. Meade, *J. Am. Chem. Soc.*, 2011, **133**, 16346–16349.
13 V. Kubíček, J. Rudovský, J. Kotek, P. Hermann, L. Vander Elst, R. N. Muller, Z. I. Kolar, H. T. Wolterbeek, J. A. Peters and I. Lukeš, *J. Am. Chem. Soc.*, 2005, **127**, 16477–16485.
14 C. Larsen, J. Ostergaard, S. W. Larsen, H. Jensen, S. Jacobsen, C. Lindegaard and P. H. Andersen, *J. Pharm. Sci.*, 2008, **97**, 4622–4654.
15 N. Gerwin, C. Hops and A. Lucke, *Adv. Drug Delivery Rev.*, 2006, **58**, 226–242.
16 N. Butoescu, O. Jordan and E. Doelker, *Eur. J. Pharm. Biopharm.*, 2009, **73**, 205–218.
17 C. Chu, A. Williams, C. Coyle and M. Bowers, *Arthritis Res. Ther.*, 2012, **14**, 1–10.
18 K. Bloecker, A. Guermazi, W. Wirth, O. Benichou, C. K. Kwoh, D. J. Hunter, M. Englund, H. Resch and F. Eckstein, *Osteoarthr. Cartil.*, 2013, **21**, 419–427.
19 F. Eckstein, G. Ateshian, R. Burgkart, D. Burstein, F. Cicuttini, B. Dardzinski, M. Gray, T. M. Link, S. Majumdar, T. Mosher, C. Peterfy, S. Totterman, J. Waterton, C. S. Winalski and D. Felson, *Osteoarthr. Cartil.*, 2006, **14**, 974–983.

20 K. Gelse, S. Söder, W. Eger, T. Diemtar and T. Aigner, *Osteoarthr. Cartil.*, 2003, **11**, 141–148.
21 P. M. van der Kraan and W. B. van den Berg, *Osteoarthr. Cartil.*, 2007, **15**, 237–244.
22 J. D. Freedman, H. Lusic, M. Wiewiorski, M. Farley, B. D. Snyder and M. W. Grinstaff, *Chem. Commun.*, 2015, **51**, 11166–11169.
23 F. W. Roemer, C. K. Kwoh, M. J. Hannon, D. J. Hunter, F. Eckstein, Z. Wang, R. M. Boudreau, M. R. John, M. C. Nevitt and A. Guermazi, *Radiology*, 2015, **274**, 810–820.
24 T. E. McAlindon, M. Nuite, N. Krishnan, R. Ruthazer, L. L. Price, D. Burstein, J. Griffith and K. Flechsenhar, *Osteoarthr. Cartil.*, 2011, **19**, 399–405.
25 M. Pickarski, T. Hayami, Y. Zhuo and T. Duong le, *BMC Musculoskeletal Disord.*, 2011, **12**, 197.
26 F. H. Chen, K. T. Rousche and R. S. Tuan, *Nat. Clin. Pract. Rheumatol.*, 2006, **2**, 373–382.
27 D. A. Rothenfluh, H. Bermudez, C. P. O'Neil and J. A. Hubbell, *Nat. Mater.*, 2008, **7**, 248–254.
28 H.-Y. Hu, N.-H. Lim, D. Ding-Pfennigdorff, J. Saas, K. U. Wendt, O. Ritzeler, H. Nagase, O. Plettenburg, C. Schultz and M. Nazare, *Bioconjugate Chem.*, 2015, **26**, 383–388.
29 K. Inagawa, T. Oohashi, K. Nishida, J. Minaguchi, T. Tsubakishita, K. O. Yaykasli, A. Ohtsuka, T. Ozaki, T. Moriguchi and Y. Ninomiya, *Osteoarthr. Cartil.*, 2009, **17**, 1209–1218.
30 T. Irie, K. Oda, A. Shiino, M. Kubo, S. Morikawa, N. Urushiyama, S. Aonuma, T. Kimura, T. Inubushi, T. Oohashi and N. Komatsu, *MedChemComm*, 2013, **4**, 1508–1512.
31 M. Woods, Z. Kovacs, S. Zhang and A. D. Sherry, *Angew. Chem., Int. Ed.*, 2003, **42**, 5889–5892.
32 E. A. Weitz, J. Y. Chang, A. H. Rosenfield, E. A. Morrow and V. C. Pierre, *Chem. Sci.*, 2013, **4**, 4052–4060.
33 J.-A. Park, J.-J. Lee, J.-C. Jung, D.-Y. Yu, C. Oh, S. Ha, T.-J. Kim and Y. Chang, *ChemBioChem*, 2008, **9**, 2811–2813.
34 R. Napolitano, T. C. Soesbe, L. M. de León-Rodríguez, A. D. Sherry and D. G. Udugamasooriya, *J. Am. Chem. Soc.*, 2011, **133**, 13023–13030.
35 A. Williams, L. Sharma, C. A. McKenzie, P. V. Prasad and D. Burstein, *Arthritis Rheumatol.*, 2005, **52**, 3528–3535.
36 S. Aime, A. Barge, J. I. Bruce, M. Botta, J. A. K. Howard, J. M. Moloney, D. Parker, A. S. de Sousa and M. Woods, *J. Am. Chem. Soc.*, 1999, **121**, 5762–5771.
37 A. Pasha, G. Tircsó, E. T. Benyó, E. Brücher and A. D. Sherry, *Eur. J. Inorg. Chem.*, 2007, **2007**, 4340–4349.
38 G. H. Simon, J. von Vopelius-Feldt, M. F. Wendland, Y. Fu, G. Piontek, J. Schlegel, M.-H. Chen and H. E. Daldrup-Link, *J. Magn. Reson. Imaging*, 2006, **23**, 720–727.
39 A tube filled with a 10 mM solution of $GdCl_3$ in DPBS was taped in the middle of two legs and served as a standard for signal intensity. This standard was used to quantify and amount of Gd^{3+} in the knee and to normalize the signal for different rats. After acquiring the control images, 50 μL of a 10 mM solution of TCA and NCA in DPBS was individually injected intra-articularly into the joint space of the two knees of one rat ($n = 4$) and post contrast images were taken immediately and followed for 3 days for studies the kinetics of the signal enhancement. For details of MRI imaging and region-of-interest (ROI) analysis, see the ESI Fig. S4.†
40 P. S. Emrani, J. N. Katz, C. L. Kessler, W. M. Reichmann, E. A. Wright, T. E. McAlindon and E. Losina, *Osteoarthr. Cartil.*, 2008, **16**, 873–882.
41 F. W. Roemer, A. Guermazi, J. Niu, Y. Zhang, A. Mohr and D. T. Felson, *Arthritis Rheumatol.*, 2012, **64**, 429–437.
42 M. B. Kinds, A. C. A. Marijnissen, M. A. Viergever, P. J. Emans, F. P. J. G. Lafeber and P. M. J. Welsing, *J. Rheumatol.*, 2013, **40**, 891–902.